J Clust Sci (2017) 28:2369–2400
DOI 10.1007/s10876-017-1256-3

REVIEW PAPER

Synthetic Study and Merits of Fe_3O_4 Nanoparticles as Emerging Material

Saba Jamil[1] · Muhammad Ramzan Saeed Ashraf Janjua[2,3]

Received: 26 May 2017 / Published online: 26 June 2017

Abstract Iron (III) oxide magnetic nanoparticles have provided us a multitude of new tools to explore biological and other scientific systems on small length scales. The opening up of single cell or single molecule phenomena to experimental investigations present an important step forward and promises to yield new insights. This review depicts some important and most commonly used methodologies for the engineering of iron oxide magnetic nanoparticles including superparamagnetic iron oxide nanoparticles and ultra-small superparamagnetic iron oxide nanoparticles, important features of these synthesis methods and their applications in different fields of life proving it as an emerging material. Most important task in nanoscale synthesis of iron oxide is to control morphology and contain it within a narrow size distribution. These processes include sol–gel method, hydrothermal method, sonochemical method, co-precipitation and micro emulsion methods. These processes are essentially highly controlled to fabricate the desire material with appropriate properties. Synthesis of mono disperse nanometer-sized magnetic particles of metal alloys and metal oxides is an active research area because of their potential technological ramifications ranging from ultrahigh-density magnetic storage media, to biological imaging. Size, size distribution, shape, and dimensionality are important for the properties of these magnetic materials. Nanoparticles of various iron oxides (Fe_3O_4 and ç-Fe_2O_3 in particular) have been widely used in a range of biological applications. Iron oxide magnetic nanoparticles can be designed to exhibit

✉ Saba Jamil
Saba_Hrb@yahoo.com

✉ Muhammad Ramzan Saeed Ashraf Janjua
Janjua@kfupm.edu.sa; Janjua@uos.edu.pk

[1] Super Light Materials and Nanotechnology Laboratory, Department of Chemistry, University of Agriculture, Faisalabad 38000, Pakistan

[2] Department of Chemistry, King Fahd University of Petroleum and Minerals (KFUPM), Dhahran 31261, Kingdom of Saudi Arabia

[3] Department of Chemistry, University of Sargodha, Sargodha 40100, Pakistan

novel and significantly improved physical, chemical and biological properties, phenomena and strategies as a result of the limited size of their constituent particles.

Graphical Abstract Iron oxide nanoparticles can be designed to exhibit novel and significantly improved physical, chemical and biological properties, phenomena and strategies as a result of the limited size of their constituent particles by using various methodologies.

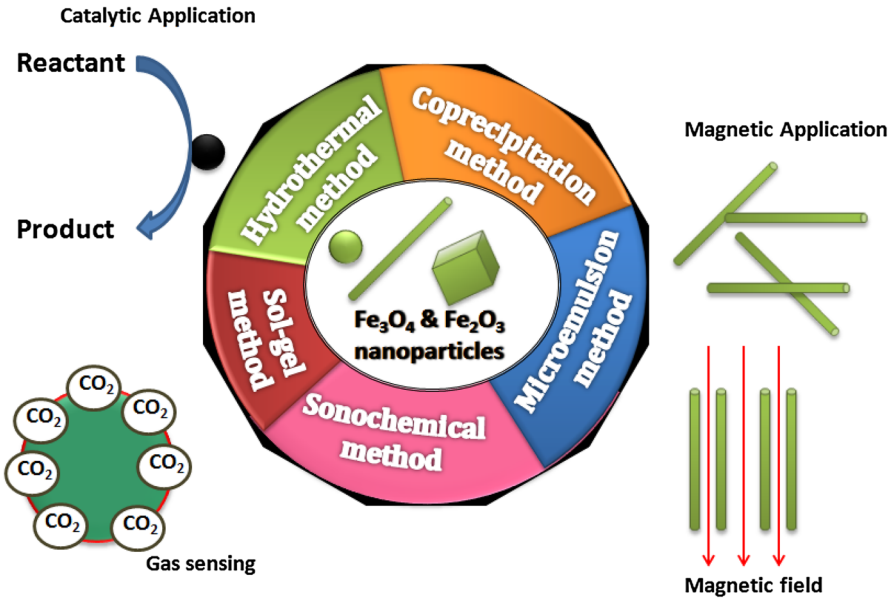

Keywords Nanomaterials · Nanoparticles · SPIONs · Magnetic · Synthesis · Applications · Emerging material

Introduction

Magnetic Nano spheres compromise attractive prospects in diverse fields of life due to their well-regulated size and magnetic properties [1]. Iron oxide magnetic nano spheres incline to be either paramagnetic or superparamagnetic with a size fluctuating from a few nanometers up to tens of nanometers. Magnetic nanoparticles are of pronounced curiosity for investigators from a wide range of disciplines, comprising magnetic fluids [2], catalysis [3, 4], biotechnology/biomedicine [5], magnetic resonance imaging [6, 7], data storage, [8] and environmental remediation [9, 10]. Functionalized nanoparticles are commonly used in catalysis, bio labeling, and bio separation [11]. Specifically in liquid-phase catalytic reactions, such small and magnetically separable particles may be useful as quasi homogeneous systems that combine the advantages of high dispersion, high reactivity, and easy separation [12]. The magnetic nanoparticles should also have high magnetic moment, and can be improved via surface chemistry reactions so that they are proficient of binding

precisely to the biomolecules of interest and able to hold out numerous physiological conditions [12]. These nanoparticle materials often display very stimulating electrical, optical, magnetic, and chemical properties, which cannot be attained by their bulk counterparts [13]. Nanosized particles have physical and chemical properties that are characteristic of neither the atom nor the bulk counterparts [14]. Quantum size elects and the large surface area of magnetic nanoparticles radically change some of the magnetic properties and exhibit superparamagnetic phenomena and quantum tunneling of magnetization [15].

Superparamagnetic iron oxide structures have the general formula $Fe_2^{3+}O_3M^{2+}O$, where M^{2+} is a divalent metal on like iron, nickel, cobalt etc. SPIO is magnetite if metal ion is ferrous ion. Superparamagnetic behavior occurs when crystals containing region of unpaired spin, are sufficiently large as they can be regarded as thermodynamically independent, single domain particles. Such particles process an overall magnetic dipole that is larger when compared to its unpaired electrons individually. In the absence of an applied magnetic field, and let the particles to rotate freely from a thermal motion of time scale that is shorter as compare to its time of observation. Ensembles of such particles are randomly oriented with no net magnetic field. However, an external magnetic field causes the magnetic dipole of the particles to reorient analogues to paramagnetic materials. The magnetic moment of such particles reflects the domain of interacting electrons that results in the form of magnetic moment greater than that of a paramagnetic substance. These single domain particles are named as magnetic domains [16–19].

In order to attain high throughput and high accuracy in bioscreening [20], the core MNPs must be rather large and their size should be precisely controlled with several dozen nanometers [21]. The stability of electronic and high density data storage devices made of magnetic nanoparticles is limited by their superparamagnetic transition [22]. Therefore, here is strong interest to understand the magnetization processes in the superparamagnetic region [23]. The current efforts are aimed at increasing the thermal energy barrier against the magnetic reversal in magnetic nanocomposite [24]. For applicability of magnetic nanoparticles it is also important to know, how the inter-particles interaction affects the physical properties of magnetic nanoparticles system [25]. The nanoparticles samples may exhibit glassy dynamics due to strong dipolar inter-particle interaction [26], but weak or non-interacting nanoparticles systems were observed after embedding into isolated matrix [6].

All these biomedical and bioengineering applications require that these nanoparticles have high magnetization values and size smaller than 100 nm with overall narrow particle size distribution, so that the particles have uniform physical and chemical properties [27–30]. In addition, these applications need special surface coating of the magnetic particles, which has to be not only non-toxic and biocompatible but also allow a targetable delivery with particle localization in a specific area [28–31]. To this end, most work in this field has been done in improving the biocompatibility of the materials, but only a few scientific investigations and developments have been carried out in improving the quality of magnetic particles, their size distribution, their shape and surface in addition to characterizing them to get a protocol for the quality control of these particles [32].

This review article deals with basic and general synthesizing routs for Fe_3O_4 and superparamagnetic iron oxide nanoparticles, and their applications in different fields. An outlook toward this emerging material reveals its dynamic contribution to society as well as science proving it a versatile material in different walks of life. In this article our main focus is on the simple Fe_3O_4 nanoparticles and superparamagnetic iron oxide nanoparticles [34].

Fe_3O_4 Magnetic Oxide Nanoparticles as an Emerging Material

Magnetite and maghemite nanoparticles are commonly studied magnetic iron oxides for clinical applications. The advantage of using iron oxide nanoparticles relies on their chemical stability in contrast to that of commonly used nanoparticles of pure Fe metal [32].

Methods of Preparation

To date, many approaches including reverse micelles method [35] and thermal decomposition route [32, 36–41] have been developed for the preparation of iron oxide nanoparticles. Wet-chemical syntheses, such as co-precipitation, sol–gel, hydrothermal and micro-emulsion techniques and a supercritical fluid [42] technique effectively control the morphology and chemical composition of prepared powders [43]. Particle synthesis by gel to crystalline conversion method helps to obtain final products at temperatures around 100 °C [44]. This method differs from the traditional sol–gel technique in two aspects: (1) no expensive alkoxide reactants are required, and (2) no need of higher temperature calcinations to produce final product [45–47]. Gold-coated iron oxide magnetic nanoparticles with a specific magnetic moment of 145 emu/g and a coercivity of 1664 Oe are being most intensively used for biomedical applications due to good corrosion resistance [48].

The synthesis of magnetic nanoparticles, covering a wide range of compositions and tuneable sizes, has made substantial progress, especially over the past decade [31]. Different kinds of monodisperse spherical nanocrystals with controllable particle sizes and compositions have been synthesized by a wide range of chemical synthetic procedures [49]: coprecipitation, reactions in constrained environments, thermal decomposition of metal–surfactant complexes, sol–gel reactions, polyol processes, flow injection synthesis, sonolysis, and electrochemical and aerosol methods [50].

Sol–Gel Method

Sol–gel methods, which have been found to be effective for dispersing small metal and oxide particles in nonmetallic matrixes, were also proposed for the preparation of iron magnetic oxide nanoparticles. Iron oxide-based porous solids were prepared by a sol–gel process using Fe(III) salts in various solvents [51].

Sol–gel methods generally refer to the hydrolysis and condensation of metal alkoxides or alkoxide precursors, leading to dispersions of oxide particles in a ''sol''. The ''sol'' is then dried or ''gelled'' by solvent removal or by chemical reaction [52]. The solvent used is generally water, but the precursors can also be hydrolyzed by an acid or base. Basic catalysis induces the formation of a colloidal gel, whereas acid catalysis yields a polymeric form of the gel [53]. The rates of hydrolysis and condensation are important parameters that affect the properties of the final products. Smaller particle sizes are obtained at slower and more controlled hydrolysis rates. The particle size also depends on the solution composition, pH, and temperature [53–56].

The rates of hydrolysis and condensation are important parameters that affect the properties of the final products [31]. Smaller particle sizes are obtained at slower and more controlled hydrolysis rates. The particle size also depends on the solution composition, pH, and temperature [24]. This compares with bulk maghemite values of 74–76 emu/g [57]. The low magnetization values suggest that the aerogels may not be suitable for magnetic applications, although they may still be useful in catalysis and other applications [58]. Disadvantages of the sol–gel methods include contamination from byproducts of reactions, as well as the need for post-treatment of the products [59].

In a typical experiment, 0.65 g of $Fe(NO_3)_3{\cdot}9H_2O$ (1.6 mmol) was dissolved in 3.5 mL of 200 proof ethanol to give a clear red–orange solution that remained unchanged upon storage, under room conditions, for several months. If, instead, a 1.0 g portion of propylene oxide was added to the solution, there was rapid (<1 min color change as the solution became an intense dark red-brown color [25]. With the passage of time, the solution is transformed into a rigid red-brown gel. Gel formation usually occurred within several minutes [46, 60–62].

Aerogel samples were processed in a Polaron supercritical point drier. The solvent liquid in the wet gel pores was exchanged for CO_2(l) for 3–4 days, after which the temperature of the vessel was ramped up to 45 °C, while maintaining a pressure of 100 bar [47]. The vessel was then depressurized at a rate of 7 bar/h approximately. For aerogel processing we preferred to use polyethylene vials to hold the gels during the extraction process [44]. This was done because much less monolith cracking was observed than when Fe_2O_3 gels were processed in glass vials. Xerogel samples were processed by drying in a fume hood at room temperature for 14–30 days. Under these conditions high vapor pressure solvents, like ethanol, were evaporated, and the wet gels were converted to xerogels [63–65].

Co-precipitation

In the co-precipitation process, two stages are involved: [32–37] a short burst of nucleation occurs when the concentration of the species reaches critical supersaturation, and then, there is a slow growth of the nuclei by diffusion of the solutes to the surface of the crystal. To produce monodisperse iron oxide nanoparticles, these two stages should be separated; i.e., nucleation should be avoided during the period of growth [51, 66–68]. Size control of monodispersed particles must normally be performed during the very short nucleation period, because the final particle number

is determined by the end of the nucleation and it does not change during particle growth [69–71]. A wide variety of factors can be adjusted in the synthesis of iron oxide nanoparticles to control size, magnetic characteristics, or surface properties. A number of studies have dealt with the influence of these different factors. According to the thermodynamics of this reaction, complete precipitation of Fe_3O_4 should be expected at a pH between 8 and 14, with a stoichiometric ratio of 2:1 (Fe^{3+}/Fe^{2+}) in a non-oxidizing oxygen environment [52].

The Fe_3O_4 magnetic nanoparticles were prepared based on the co-precipitation of Fe^{3+} and Fe^{2+} under the aqueous ammonia (0.3 mol L^{-1}) as precipitating agent. Briefly, ferrous chloride tetrahydrate and ferric chloride are dissolved in 100 ml deionized water were under vigorous stirring and with the protection of nitrogen to prepare total concentration of 0.015 mol-L^{-1} ferrite solution containing 1 g PEG4000 emulsifier. Aqueous ammonia (0.3 M) was dropped slowly into the mixture solution until the pH value was titrated to 11.0 [72]. It can be observed that the solution became black due to the formation of Fe_3O_4 particles. The sample was kept reacting in water bath at 50 °C for 30 min under vigorous stirring and dispersed in ultra sonicator for another 30 min. The black mixture was then aged at 80 °C for 1 h. After that, the product prepared was transferred to a large beaker and dissociated from liquor with the ferromagnet. Finally, the Fe_3O_4 magnetic nanoparticles were washed with distilled water until the pH value descended to 7.0, and were collected in vacuum drying chamber after being dried for 4 h at 60 °C. The main advantage of the co-precipitation process is that a large amount of nanoparticles can be synthesized. However, the control of particle size distribution is limited, because only kinetic factors are controlling the growth of the crystal [72–77].

Facile Hydrothermal Synthesis of Iron Oxide Nanoparticles

Hydrothermal synthesis is generally defined as crystal synthesis or crystal growth under high temperature and high pressure water conditions from substances which are insoluble in ordinary temperature and pressure (<100 °C, <1 atm). Since ionic product equilibrium (Kw) has a maximum value of around 250–300 °C, hydrothermal synthesis is usually carried out below 300 °C. The critical temperature and pressure of water are 374 °C and 22.1 MPa, respectively [78].

In a typical synthesis, $FeCl_2{\cdot}4H_2O$ (0.25 g) was dissolved in 12.75 mL water. Under vigorous stirring, ammonium hydroxide (1.25 mL) was added, and the suspension was continuously stirred in air for 10 min, allowing the iron(II) to be oxidized. The reaction mixture was then autoclaved in a sealed pressure vessel with a volume of 48 mL at 134 °C for 3 h under air with a gauge pressure of 2 bar and cooled down to room temperature. The black precipitate was collected and purified with water via a centrifugation-dispersion process. The final Fe_3O_4 NP suspension was lyophilized to obtain black dry powder [79]. The process of formation of nanospheres by this method is given as Fig. 1.

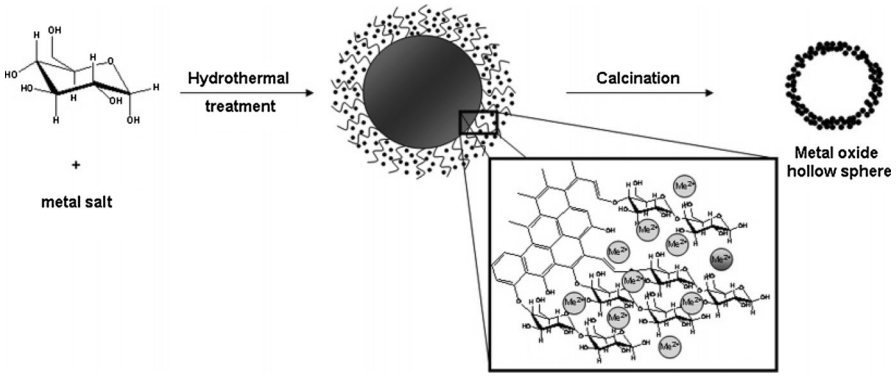

Fig. 1 Diagrammatical illustration of mechanism of formation of metal oxide hollow nanospheres by hydrothermal approach [80]

Batch Hydrothermal Synthesis

In the batch reaction system, one of the advantages for synthesis of metal oxides in supercritical water is reducing alkaline concentration for the crystal phase formation [81].

In the batch synthesis of Fe_2O_3 gel, hydrated iron (III) chloride ($FeCl_3{\cdot}6H_2O$) was used as the precursor and 1,2-epoxybutane was used as the complexing agent. Alcohol was used as the solvent, and water was used as the gelation agent. $FeCl_3{\cdot}6H_2O$ (1.25 g) was added to 40 mL of absolute ethanol in a beaker and ultrasonicated for 20 min to obtain a clear yellow solution. To this mixture, 5 mL of epoxide and 1 mL of water were simultaneously added and the solution was stirred. The mixture was then allowed to sit until the solution formed a gel (time at which the solution could no longer flow). In the process of gel formation, the color of the solution gradually changes to reddish brown and the viscosity increases [55]. The morphology of the product obtained by hydrothermal/solvothermal method is given in Fig. 2.

Solvothermal Synthesis

In this type of synthesis any other type of organic, inorganic or ionic liquids can be used as solvent replacing the water that is basic in hydrothermal process [83].

In a typical synthesis, into 13.0 mL (0.223 mol) of absolute ethanol 0.121 g (0.3 mmol) of $Fe(NO_3)_3{\cdot}9H_2O$ was dissolved to form a dark red solution, and into it 1.3 g (0.024 mmol) of PVP (Mw = 58,000) was added under magnetic stirring. With the PVP dissolving, the solution gradually transformed into a viscous sol, which was poured into a Teflon-lined autoclave and heated at 240 °C for 4.0 h. After that the autoclave was cooled to room temperature, the as-obtained black suspension was mixed with an equal volume of ethanol, and the formed precipitate (γ-Fe_2O_3) was separated by centrifugation at 9500 rpm and washed with ethanol. Then it was redispersed into 13.0 mL (0.082 mol) of n-octanol to form a solution,

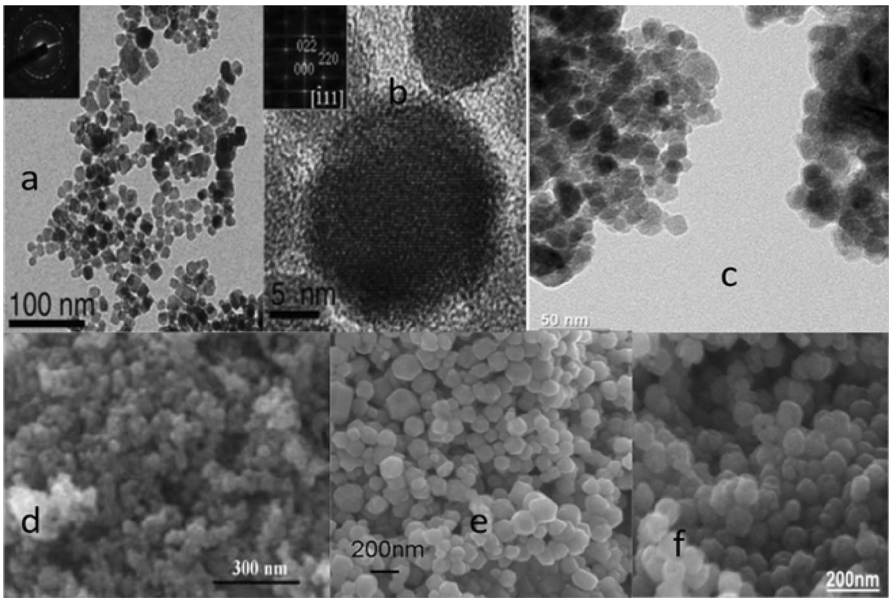

Fig. 2 Morphology of the iron oxide nanoparticles obtained by different hydrothermal strategies [82]

and into it 0.5 g (8.6×10^{-3} mmol) of PVP and 0.2 mL (3.2 mmol) of hydrazine hydrate (80%) were added under stirring to form a homogeneous sol, which was transferred to an autoclave and heated a 180 °C for 6.0 h. After that the product (Fe_3O_4) was collected by centrifugation and washed with ethanol [84].

Green Synthesis of Nanoparticles

The use of toxic chemicals and non-polar solvents in synthesis limits the use of nanoparticles in clinical fields. Thus, it is needed to develop a clean, non-toxic, biocompatible and eco-friendly method for the synthesis of nanoparticles. Microbial synthesis of nanoparticles is a green chemistry approach that connects the fields of nanotechnology and microbial biotechnology. Biological synthesis of gold, silver, gold–silver alloy, platinum, palladium, selenium, tellurium, silica, titania, zirconia, magnetite and uraninite particles by bacteria, actinomycetes, fungi and yeasts have been reported worldwide [85]. Even though biological synthesis of nanoparticles is considered cost effective, safe, environment-friendly and sustainable, it has various drawbacks. The culturing of microorganisms is time-consuming and it is difficult to have fine control over shape, size and crystallinity. The particles are not monodisperse and the rate of production is slow. These are the various problems which have vexed the biological synthesis of nanoparticles. But optimization of factors involved like pH, temperature, metal ion concentration, and the strain of the microbe used has given hope for large scale application of biological synthesis. Moreover genetically engineered strains which express the reducing agent maximally can be used in the future which will provide better control over the

shape and size of nanoparticles [86]. An example of green synthesis is biopolymer-assisted green synthesis of iron oxide nanoparticles.

Biopolymer-Assisted Green Synthesis of Iron Oxide Nanoparticles

To prepare Fe_3O_4 nanoparticles, 0.5 g of urea was added to 10 mL of aqueous solution containing 1.5 mmol of $FeCl_3$, which was followed by the dropwise addition of 25 mL of a 25.4 mm sodium alginate aqueous solution (calculated by the repeating unit). Subsequently, the resulting solution was transferred into a 50 mL Teflon-lined autoclave and heated at 453 K for 24 h. A black solid product were collected, and then washed with distilled water several times, and finally dried in air [87].

Micro Emulsion

Microemulsion is a thermodynamically stable isotropic dispersion of two immiscible phases (water and oil) under the surfactant present, the surfactant molecules may form a monolayer at the interface between the oil and water, with the hydrophobic tails of the surfactant molecules dissolved in the oil phase and the hydrophilic head groups in the aqueous phase [87–91]

Water-in-oil (w/o) microemulsions consisting of nanosized water droplets dispersed in an oil phase and stabilized by surfactant molecules at the water/oil interface have been widely used to obtain iron oxide nanoparticles [92]. The surfactant-covered water pools offer a unique microenvironment for the formation of nanoparticles and for limiting their growth [93]. The size of the microemulsion droplets is determined by the water to surfactant ratio, although the eventual size of the nanoparticles may also be influenced by factors such as concentration of reactants (especially surfactant) and flexibility of the surfactant film [56, 94, 95].There are several ways to utilize microemulsions to produce nanoparticles. In one method, reactants A and B are dissolved in the aqueous phases of two identical w/o microemulsions and form an AB precipitate upon mixing (see Fig. 3a) [31]. In another method, nanoparticles are produced by the addition of a reducing or precipitating agent to a microemulsion containing the primary reactant dissolved in an aqueous phase (Fig. 3b). The reducing or precipitating agent can be a liquid such as hydrazine or a gas such as hydrogen [96]. Figure 3 depicts another method for the formation of oxide, hydroxide or carbonate precipitates by bubbling gases like O_2, NH_3, or CO_2 through a microemulsion containing soluble salts of the cations [97].

Iron oxide nanoparticles were prepared by microemulsion mediated synthesis process [24]. This synthesis process was carried out at room temperature. The preparation of iron oxide nanoparticles was performed according to the following procedure. Ferrous chloride salt solution was prepared at a concentration of 0.2 M. The $FeCl_2$ solution was stabilized by addition of a few drops of 0.5 M hydrochloric acid. 0.25 M NaOH salt solution was then prepared. Then, the microemulsion was prepared by dissolving HTAB in n-octane, followed by addition of 1-butanol and then $FeCl_2$ aqueous salt solution. The system was stirred slowly until a transparent

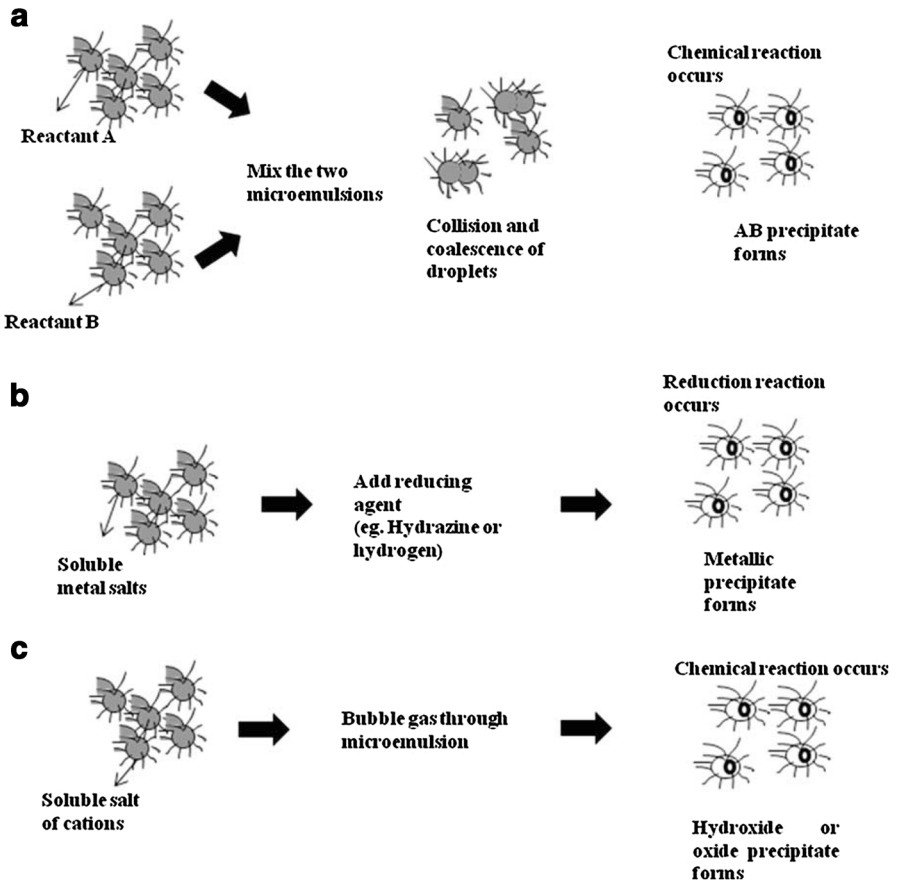

Fig. 3 Schematic illustration of iron oxide nanoparticles prepared by micro emulsion mediated synthesis process [97–99]

microemulsion suspension was obtained. The steps above were repeated to produce the second microemulsion that contained 0.25 M NaOH solution. This two microemulsion systems were then mixed at a volumetric ratio of 1:1. Immediately, a dark green precipitate was formed. It then transformed to black. The particles were recovered and then washed several times with deionized water and acetone. They were dried at room temperature and named as S1. The same procedure was repeated to produce a second sample with initial Fe^{2+} concentration of 0.1 M. The NaOH concentration was maintained at 0.25 M. The volumetric ratio of micoremulsion containing Fe^{2+} to microemulsion containing OH^{-} was 2:1. This causes an increase of the total number of microemulsions [100]. The morphology of the product prepared by microemulsion method is described in Fig. 4.

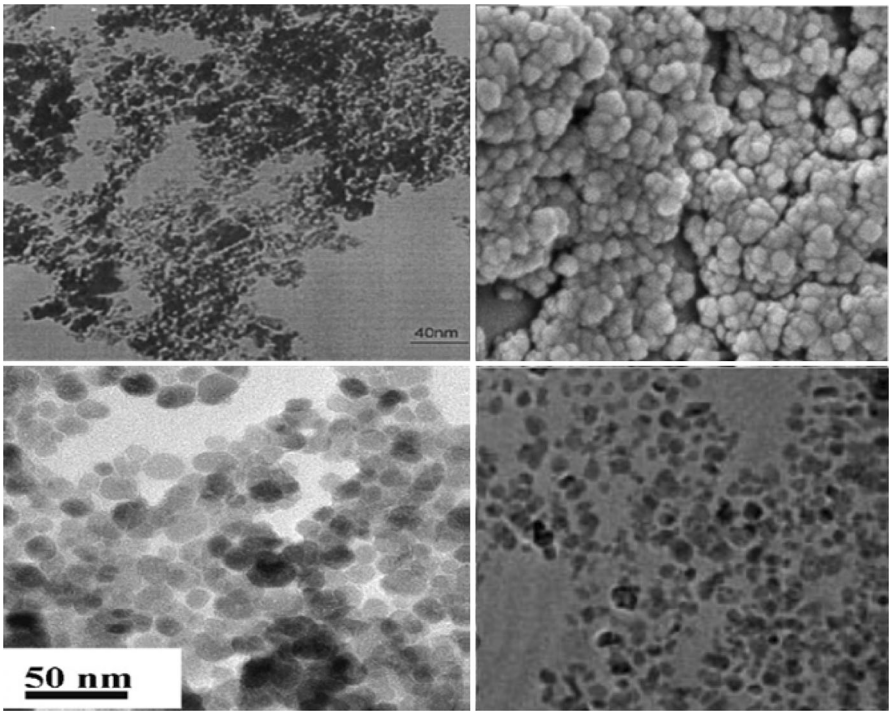

Fig. 4 Morphology of iron oxide magnetic nanoparticles obtained by micro emulsion method [57, 101, 102]

Sonochemical Synthesis

As a competitive alternative, the sonochemical method has been extensively used to generate novel materials with unusual properties [58]. This method has been applied for the synthesis of various nanocomposites, and its versatility has been successfully demonstrated in iron oxide nanoparticles preparation [59]. The prepared Fe_3O_4 nanoparticles are superparamagnetic and its magnetization at room temperature is very low (1.25 emu/g) [25, 60, 103].

Although Fe_3O_4 has been synthesized through different approaches [24], the chemical co-precipitation process is the most common. However, in most cases, the particles formed are only just within the micrometer scale [104], and it is difficult to control the size distribution and scale in an ordinary chemical co-precipitation process [105]. The rapid progress of microelectronic technology and other fields of industry require continuous reduction of component size, stimulating the demand for synthesis of ultra-fine particles and functional materials. Much attention has been paid to ultrasound/chemical (sonochemical) methods for the production of nanomaterials [106]. The transmission of ultrasound in a liquid phase provides mixing conditions favorable for chemical reaction, and generates transient extreme temperature or high shear-rate through acoustic cavitations, which has a specific

effect on a chemical reaction that is very suitable for the formation of nanoparticles. Several kinds of nanoparticles have been synthesized by this method [107].

The advantage of sonochemical synthesis is that one can obtain atomic level mixing of the constituent ions in the amorphous phase so that the crystalline phase can be obtained by annealing at relatively low temperatures [108]. The cavitation is a quenching process, and hence the composition of the particles formed is identical to the composition of the vapor in the bubbles, without phase separation [109].

$$2\mathrm{Fe(III)} + \mathrm{Fe(II)} + 8\mathrm{OH}^- \rightarrow \mathrm{Fe_3O_4} + 8\mathrm{H_2O}$$

A freshly prepared mixture of 1.5 mmol $FeCl_3{\cdot}6H_2O$ (97%, Aldrich) and 0.75 mmol $FeCl_2{\cdot}4H_2O$ (99%, Aldrich) in 5 mL of 0.05 M HCl was rapidly injected via a fine plastic tube to 40 mL of 2 M ammonia solution containing 0.01 M of hydrazine (98%, Aldrich) under power ultrasound at 3032 °C in an argon flow [110]. Hydrazine reduced the redox potential of solution preventing Fe(II) from oxidizing. The injection was performed into the active zone of the sonoreactor via a fine plastic tube. Solids with a distinctive black color of magnetite were precipitated immediately after injection [111, 112]. The mixture was sonicated for 5 min. The sediment was transferred to a nitrogen filled glovebox, separated with a permanent magnet, and washed twice with argon purged 0.1 M [113–117]. Flow sheet diagram for the sonochemical method of synthesis is given in Fig. 5.

The sonochemical method requires expensive organometallic compounds as precursors, but offers better control of the size and size distribution of particles [119]. This facile synthetic process would be advantageous for the laboratory scale production of Fe_3O_4 nanoparticles having uniform morphology and narrow size distribution [120]. A comparison of nanoparticles obtained by different methods is given as Table 1.

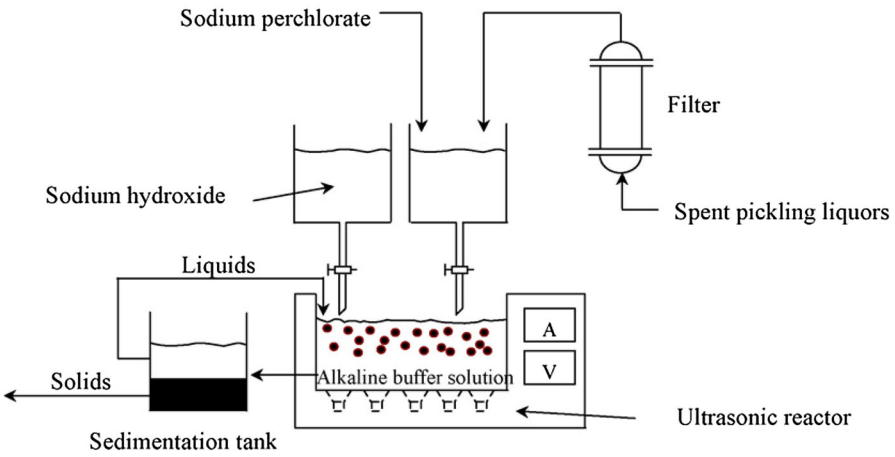

Fig. 5 Flow sheet diagram for the sonochemical method [118]

Table 1 Comparison between different approaches for the synthesis of iron oxide magnetic nanoparticles [121]

	Hydrothermal synthesis	Sonochemical synthesis	Co-precipitation	Sol–gel method	Micro emulsion method
Size and size distribution	About 12–40 nm	2–40 nm broad size distribution	About 10–50 nm with broad size distribution	About 20–200 nm with broad size distribution	About 4–15 nm with very narrow size distribution
Morphology	Spherical	Spherical Cuboid Aggregates	Spherical (large aggregates)	Spherical with high porosity	Cubic or spherical (no aggregation)
Magnetization values	85.8 emu/g Depend on size	1–2 emu/g	20–50 emu/g with super paramagnetic behaviour	10–40 emu/g with paramagnetic behavior	430 emu/g with Super paramagnetic behavior
Advantages	Controlled size and shape, dislocation-free single crystal particles better grain crystallinity	Useful for protective coatings and thin film deposition	Water-soluble and biocompatible iron oxide NPs	Particles of desired shape and length can be synthesized, useful making hybrid nanoparticles	Uniform properties and also size of the nanoparticles can be modulated
Disadvantages	Need of expensive autoclaves, and the impossibility of observing the crystal as it grows	Require very high Temperatures	Low control of the particle shape, broad distributions of sizes and aggregation of particles	Product usually contains sol–gel matrix components at their surfaces	Surfactants are difficult to remove, only a small quantities of iron oxide can be synthesized

Applications of Fe_3O_4 Nanoparticles and Superparamagnetic Iron Oxide Nanoparticles

Magnetic nanoparticles are playing an important role in a wide range of sophisticated bio-medical applications, such as targeted drug delivery [122], magnetic cell sorting and immunoassays [123], biochemical sensing [73], and ultra-sensitive disease detection [124]. Owing to its structure, magnetite is a typical semi-metallic material, which has been widely used in the fields of magnetism, photoelectric plot [125], biomedicine, high-gradient magnetic separation (HGMS) [126] and Efficient Surface-Enhanced Raman Scattering [127]. Especially, properly coated or surface- modified magnetite nanoparticles can be applied in clinical diagnosis and as a medicine transporter [128]. A complete overview of method of synthesis of nanoparticles, their size distributions and applications is given in Table 2.

Magnetite, Fe_3O_4, is a ferromagnetic material with Curie temperature of about 580 °C. It is known to be one of the most magnetic mineral with spin polarization close to 100% as per band-structure calculations. Thus, Fe_3O_4 is a promising material for many magnetic allied applications. The magnetic study of iron oxide nanoparticles provides a new insight into spin disorders and proton relaxivity that leads to imperative biomedical applications as well as in energy transfer devices [129]. The surface functionalization and modification of magnetic iron oxide NPs to bring in additional functionality is significantly important due to following reasons: (a) Improves the biocompatibility and chemical stability, and tailors the dispersibility and water solubility; (b) Endows the iron oxide new physico-chemical properties, such as magnet-optical properties, magnetic-electrical properties, magnetic-thermal properties, etc.; (c) Provides the iron oxide new functional end groups for the ensuing functionalized procedures or the subsequent applications, such as conjugation with the DNA, antibody, protein, etc. [130]. Applications avowed in this review include naked surface iron oxide magnetic nanoparticles as well as surface modified iron oxide nanoparticles.

The discovery of its gas sensing capability and applications in lithium-ion batteries has highlighted the need of a more effective fabrication approach [131]. Alignment, uniform dispersion, selective growth and diameter control are general parameters which play vital roles in the flourishing integration of nanostructures for the fabrication of bioelectronic sensing devices [132].

Success in each field has enthused multiple variations that prolong to drive the rapid evolution of the field. The high surface areas of nano structured materials are also valuable for chemical sensing [133]. Chemical sensors are extensively used for engineering process control and are experiencing growing use in security applications [134]. The nano-sized porous Fe_3O_4 particles with facile synthesis, good cycling performance and high capacity retention are promising candidate as anode materials for high energy–density lithium-ion batteries [135–137]. The magnetic Fe_3O_4 particles for the optimized DNA extraction procedure prove exceptional in effectiveness and it can be appropriate to extract plasmid DNA from agarose gel [138]. Fe_3O_4 novel fractal nanocrystals have been synthesized by a surfactant-assisted solvothermal process showing relatively high saturation

Table 2 A complete overview of method of synthesis of nanoparticles, their size distributions and applications

Materials: Fe_3O_4 magnetic nanoparticles, SPIONs and USPIONs					
Type of applications	Size dist.	Method	Advantages	Uses	Refs.
Bio-sensors					
SPR	32.82, 14.51 nm	Pyrolysis/spherical aggregates	Biocompatible. Efficient	Sensor for DNA bases	[157]
Volta metric Sensing of dopamine	10 nm	Hydrothermal/spherical aggregates	Excellent sensitivity and recovery, strong promoting effect and high stability toward the electrochemical oxidation of dopamine (DA), reproducibility	Voltammetric sensing	[158]
Electro catalytic reduction of H_2O_2	8 nm after modification 12 nm	Co-precipitation/oval to sphere, Irregular	Chemical modified electrode effectively catalyzes the reduction of H_2O_2	Biosensor without mediator	[159]
Sensor	7 nm	Co-precipitation/spherical	Enhance signal for GMR sensors	Sensor for small biomolecules	[160]
Glucose biosensor	20 nm	Co-precipitation/spherical	Relatively rapid response, high sensitivity, broad linear range, low detection limit, good reproducibility, and long term stability	Glucose detection of clinically important antigens	[161]
Tyrosinase bio sensor	30 nm	Ultra-sonication/compact globe shape	Rapid, simple, and cost-effective analysis of phenolic contaminants in environmental samples	Detect catechol, enzyme-based biosensors, determining phenolic compounds	[162]
Sol–gel/chitosan biosensor	5.48 ± 1.37 nm	Hydrothermal/cluster like structure, some are fine	Pathway for electron transfer improved the conductive properties	Determination of the herbicide 2, 4-D and heavy metals HPLC method	[163]
Enzyme based bio sensor					

Table 2 continued

Materials: Fe_3O_4 magnetic nanoparticles, SPIONs and USPIONs					
Type of applications	Size dist.	Method	Advantages	Uses	Refs.
Electrochemical sensor	125 and 225 nm	Co-precipitation/spherical to irregular	Effective guanine oxidation signal generation, detect oligonucleotides quite sensitively and selectively, less time-consuming, and cheaper label free electrochemical technique	Quantification of target DNA, detection of specific DNA sequences related to inheritance, detection of genetic diseases in PCR products	[164]
Magnetic biosensor system	26–30.6 nm	Chemical co-precipitation/spherical	Bio compatible, target specific	Probing various bio-targets, detection and identification of infectious diseases in crops and livestock	[165]
Potentiometric immunosensor	20 nm	Co-precipitation/aggregates	Used expediently, renewed easily and low-cost relatively, better stability and higher sensitivity; nonlabeled and renewable	Detection of immunoglobulin G (igg], clinical diagnosis, monitoring of disease and environmental studies; analysis of serum Sample	[165]
Electrochemical Immunosensor	20 nm	Sol–gel/dumb bell like shape	A wide linear range (0.01–10 ng/mL), low detection limit (5 pg/mL), good reproducibility and stability, precision	Detection of cancer marker PSA, detection of different biomolecules, clinical analysis	[162]
Electrochemical biosensors	65 nm	Commercially purchased/spherical aggregates	Direct cyclic voltammetric responses at PG electrodes, effective electron transfer rates involving the heme Fe(III)/Fe(II). Good electrocatalytic properties	Third generation biosensor based on the direct electrochemistry of enzymes, protein immobilization detection system	[162]
SPR sensing	10.46 nm	Pyrolysis/spherical	Sufficient specificity and thrombin, identified with high selectivity	Amplification reagent for SPR based sandwich immunoassay, biodetection, biosensor, bioseparation	[166]
Magneto-impedance biosensor	30 nm	Co-precipitation/Irregular	HEK 293 cells infected by the nanoparticles, High cell uptake	development of MI magnetic field detector with a bath for fluids, chemotherapy or hyperthermia	[166]

Table 2 continued

Materials: Fe_3O_4 magnetic nanoparticles, SPIONs and USPIONs					
Type of applications	Size dist.	Method	Advantages	Uses	Refs.
Drug delivery					
Intra-cavitary drug delivery	10 nm	Massart's method/dispersed, non-agglomerated	Nontoxic to endothelial (HUVEC), epithelial (HRPE), and tumor (pc3 and c4-2) cells, biocompatible	Hyperthermia, cancer diagnosis and bio-distribution studies, and cancer therapy	[167]
Oleic acid-pleuronic stabilized magnetite drug loading system	9.3 nm	Co-precipitation/spherical	Sustained intracellular retention and dose-dependent antiproliferative activity in cancer cells. Possible to load any hydrophobic drug	Universal drug carrier system for systemic administration of water-insoluble drugs while simultaneously allowing magnetic targeting and/or imaging	[168]
Targeted-drug carriers	8–14 nm	Aqueous co-precipitation/ Cubic shaped	Stable quality, high magnetic responses and easy achievement	Magnetic carriers for further tests in targeted-drug therapy	[169]
Anticancer drug carriers	18.7 nm	Chemical co-precipitation/spherical aggregate	Sustained-release property, non toxic, biocompatible	Chemotherapy medication,embolism of blood vessels and heat treatment of magnetic fluids, target-orientation administration system	[170]
Tumor targeting and imaging					
Multi drug resistance circumvent	10–100 nm	Co-precipitation/spherical	Very high loading of DOX. circumvent the drug resistance associated with over expression of ATP-binding cassette (ABC) transporters	Effective therapy for deadly drug-resistant cancers patient	[170]
Dual imaging Probe for cancer	25.6 (2.7 nm)	Thermal cross-linking method/Spherical	Highest accumulation of the $cy_{5.5}$ TCL-SPION within the tumor, efficiently detect tumors, an enhanced permeability and retention effect	Dual (MR/optical) imaging probe for cancer in vivo, cancer imaging and therapy	[171]

Table 2 continued

Materials: Fe_3O_4 magnetic nanoparticles, SPIONs and USPIONs					
Type of applications	Size dist.	Method	Advantages	Uses	Refs.
Anticancer drug accumulation in cancer Cells	30 nm	Electrochemical deposition under oxidizing conditions (edoc) method/irregular to spherical aggregates	Effective drug concentration, synergistic enhanced effect of the drug uptake of target cancer cells, inhibit the Multidrug resistance	Relative bio recognition processes of the targeted cancer cells, chemotherapy of cancer	[171]
Immuno-labeling of cancer cells	30 nm	Chemical co-precipitation/spherical dots	Able to recognize specific cell types or organs, strong fluorescent emission and desired super paramagnetic properties	Immuno-labeling and fluorescent Imaging of HeLa cells, specific recognition of biological targets, magnetically guiding and optically tracking the delivery of drugs and genes	[172]
Tumor integrin targeting	19.3 nm	Modified pyrolysis/ Nanoplatform	High stability of the particles in the circulation, less extent of opsonization, res reorganization and elimination, excellent tumor targeting efficiency, relatively long circulation half-life and limited liver macrophage engulfment	Vascularised solid tumors targeting	[173]
In vitro Cytotoxicity Assays For Normal, Glia and Breast Cancer Cells	5 nm	Modified phase transfer/spherical	Non toxicity in the range of 0.1–10 μg mL^{-1}, biocompatibility and bio safety for In vivo use	Bio-applications such as drug delivery, magnetic resonance imaging and magnetic hyperthermia	[174]
Nano carrier system	3–15 nm	Oil-in-water emulsions/ irregular nanocrystals	Biodegradable nano carrier system, multifunctional, the ease of fabrication, the flexibility	Detection with magnetic resonance imaging (MRI), optical imaging, used as a drug delivery vehicle	[175]

Table 2 continued

Materials: Fe_3O_4 magnetic nanoparticles, SPIONs and USPIONs

Type of applications	Size dist.	Method	Advantages	Uses	Refs.
Targeted cancer therapy	6–11 nm	Co-precipitation/spherical	Sustained release of hydrophobic drugs, biocompatible	Treatment of HER2—over expressing cancer cells, chemotherapeutic drugs, potential antiproliferative effect in MCF-7, as potential drug carrier for the active therapeutic aspects in cancer therapy	[176]
Tagging of Adenovirus	5–10 nm	Thermal decomposition/ irregular to spherical	Adequate quantities for magnetically labeling viruses	MRI enhancement and magnetic hyperthemia therapy, linker to bind polyhistidine tags onto viruses	[177]
Immobilization					
BSA immobilization	10–15 nm	Controlled co-precipitation/spherical	No adverse cell reaction, no cytoskeletal disorganization, no evidence of vacuoles in the cell body, no endocytosis	Protein immobilization, enzyme immobilization	[178]
Lipase immobilization	11.2 nm	Co-precipitation/aggregated	High catalytic activity under the employed conditions, the biocatalyst loading seems to be so high for a good conversion of soybean oil, good Ph tolerance and thermo-stability	Biodiesel production, enzymatic transesterification	[179]
Immobilization of yeast alcohol dehydrogenase	10.6 nm	Co-precipitation/spherical	Considerable improvement in stability, preventing the autodigestion and/or thermal inactivation of enzyme, higher specific surface area	Protein immobilization, enzyme immobilization, improving stability of enzyme	[180]
Orthopedic applications					
Reversing osteoporosis	5–20 nm	Wet-chemical method/ irregular to rod shaped	Enhanced osteoblast density, increase bone growth at desired bone defect sites	Orthopedic applications, magnetic therapeutic systems,	[181]

Table 2 continued

Materials: Fe_3O_4 magnetic nanoparticles, SPIONs and USPIONs					
Type of applications	Size dist.	Method	Advantages	Uses	Refs.
Enhanced cell seeding into scaffolds	150 nm	Co-precipitation/spherical	Biocompatible, enhance cell-seeding efficiency, non-toxic	Tissue engineering, mag-seeding	[182]
Magnetic sorbent/adsorption					
Heavy metal remediation	10 nm	Co-precipitation/spherical aggregates	Heavy metal removal efficiency, cheap and environmentally friendly, recovering ability of absorbed metals	Removal of heavy metals from various waters like Hg(II), Pb(II), Cd(II), and Cu(II), purification of water	[183]
Removal of Cu(II) ions	13.5 nm	Co-precipitation/spherical agglomerated	High specific surface area and the absence of internal diffusion resistance	Magnetic nano-adsorbent, the magnetic carriers of enzymes, proteins, DNA, drugs	[184]
Removal of Hg_2	80–100 nm	Hydrolysis/cubic	Higher uptake efficiency for mercury	Purification of real effluents of different chemical composition, Hg_{2+} from water	[185]
Removal of metal ions from water such as Ni(II), Cu(II), Cd(II) and Cr(VI)	6–8 nm	Co-precipitation polyol method/sphere or circular rings	Extremely high adsorption capacity to the highly-distorted surface, recovery of metal ions	Waste water purification removal of metal ions detoxification, drug delivery and drug decoration	[186]
Isolation and detection of E. coli O157:H7from food	40–60 nm	Co-precipitation polyol method/roughly spherical	No cross reactivity and nonspecific binding, high specificity, fast and sensitive	Immunological method for bacteria isolation, bio analysis and bio detection	[187]

Table 2 continued

Materials: Fe_3O_4 magnetic nanoparticles, SPIONs and USPIONs					
Type of applications	Size dist.	Method	Advantages	Uses	Refs.
Uptake, translocation, and accumulation by pumpkin plants	20 nm	Co-precipitation/irregular	Biological compatibility and structural stability	Assessing the impacts of nanomaterials and nanotechnology on public health and ecological systems, non-human biota, and ecosystems imperative	[188]
Removal of amaranth (AM)	20–80 nm	Co-precipitation/irregular	High adsorption capacity, fast adsorption, desorption, high specific surface area, absence of internal diffusion resistance	Removal of the anionic dye from waste water, separation of dye	[189]
Removal of phosphorous (P)	90.6 ± 1.2 nm	Stoichiometric Co-precipitation/spherical	Remarkable increase in electrophoretic mobility. biocompatibility and low toxicity	Full-scale process for lake restoration, decreasing P external loading to aquatic ecosystems	[190]
Removal of toxicant from water	70 nm	Ethylene glycol (EG)-mediated self-assembly process/Nano petals	Excellent ability to remove various water pollutant, nontoxic	Water treatment, adsorbents or catalysts to remove organic waste from water	[172]
Fe_3O_4 magnetic nanoparticles as peroxidase mimetics	417 nm	Co-precipitation/spherical	Higher response, catalytic activity toward ABTS oxidation by H_2O_2, high selectivity towards glucose detection	H_2O_2 detection colorimetric glucose detection using GOx, biosensors	[181]
Arsenic removal	10–11 nm	Co-precipitation/nanocrystals to irregular	High binding capacity, complete (over 99.9%) arsenic removal within 1 ppb	Arsenic separation from water	[191]
Hyperthermia					
Intracellular hyperthermia treatment of solid tumors	10–20 nm	Co-precipitation/grape like organization	Overexpress the specific receptor for this vitamin, efficacy in targeting cancer cells target specificity	MRI contrast enhancement, hyperthermia mediators	[192]

Table 2 continued

Materials: Fe_3O_4 magnetic nanoparticles, SPIONs and USPIONs					
Type of applications	Size dist.	Method	Advantages	Uses	Refs.
Magnetic fluid hyperthermia	10 nm	Reverse micelle process/ irregular	Supports colloidal stabilization, enhance the specific power absorption, biocompatibility	Biological strategies, clinical hyperthermia, interventional radiology, micro-surgery, operating navigation systems, cancer treatment with AC magnetic field	[193]
Therapy for bone cancer	15 nm	Hydrothermal/aggregates trapped in rod shaped HA	Generation of high temperature, sufficient binding properties	Hyperthermia therapies for bone cancer	[194]
Cancer Immunotherapy	10–25 nm	Co-precipitation/spherical	Enhance the immune response, heat controlled necrosis with HSP expression, protects cells from apoptotic cell death	MCL-induced hyperthermia via HSP expression	[194]
Blood cancer therapy	17 nm	Chemical co-precipitation/ Spherical	Good biocompatibility, hemocompatibile, non toxic	Targeted tumor therapy, congener chemo therapeutics in clinical therapy, the treatment of hematologic malignancies	[195]
Lysozyme amyloid aggregation	23 nm	Co-precipitation/nearly spherical	Reduction of the amyloid aggregates, promoting depolymerization, low potential biological risk	Therapeutic agents against amyloid diseases and their non-risk exploitation in nanomedicine and nanodiagnostics	[195]
Gene delivery					
Three-dimensional (3D) cellular assays	25–30 nm	Co precipitation/spherical	Transfect transgenes into cells grown, modulate the expression of these transgenes with interfering RNA	RNAi screening for therapeutic applications, pathway analysis in 3D cell culture assays	[196]
Non-viral vectors for gene delivery		Co precipitation/spherical	Efficient uptake and low toxicity	protein delivery, gene delivery in vivo, proteins targeted at inhibiting joint inflammation and cartilage matrix degradation	[196]

Table 2 continued

Materials: Fe_3O_4 magnetic nanoparticles, SPIONs and USPIONs					
Type of applications	Size dist.	Method	Advantages	Uses	Refs.
Apoptosis					
C-Jun N-terminal kinase-mediated apoptosis	SPIO = 60 nm USPIO = 20 nm	Commercially purchased/spherical	Demonstrating aggravation of symptoms, enhance the expression of the stem cell transcription factor Oct-4 in human mesenchymal stem cells, rapidly taken up by macrophages, induce delayed apoptosis through the induction of ROS and subsequent JNK signaling	Cell labeling, gene expression, a suitable strategy to reduce the oxidative damage of macrophages after MRI, biomedical applications	[197]
MRI applications					
Magnetic resonance (MR) images of liver, marrow and lymph	13 nm	Modified co-precipitation/ quasi spherical	Easily detected visually, leading to high sensitivity and specificity, higher value on differentiation of malignancy from benignancy in liver, spleen, lymph nodes and bone marrow diseases	Functional molecular imaging for biomedical research and clinical diagnosis	[198]
Stabilizer for emulsion	12 nm	Hydrothermal/Anomalous spherical shape	Interfacial adsorption, sensitive to pH and ion strength	pH-responsive pickering emulsions, control of drug release, cell populations, and mineral flotation	[198]
Dual contrast agents	12–70 nm	Water-in-oil-in-water emulsion/nano spheres embed in micro bubbles	Enhance the ultrasound contrast significantly, retain the acoustic property under the ultrasound exposure, maintain adequate echogenicity	Magnetic resonance and ultrasound imaging, US contrast agents, MR studies of other organs and tissues	[198]
Theranostic nano system	15 nm	Pyrolysis/spherical	Non-toxic, biodegradable and inexpensive, massive accumulation in lesions, high extravasation rate, and low uptake of the particles by macrophages at the tumor area, a good retention rate and a high extravasation	positron emission tomography (PET)/ near-infrared fluorescence (NIRF)/magnetic resonance imaging (MRI) tri-modality imaging	[130]

Table 2 continued

Materials: Fe_3O_4 magnetic nanoparticles, SPIONs and USPIONs					
Type of applications	Size dist.	Method	Advantages	Uses	Refs.
Spin disorder and proton relaxivity system	10 and 30 nm	Solvo-thermal/nano crystals	Different levels of MRI contrast enhancement, substantial increase in proton relaxivity when hydrophobic surface ligands are replaced with hydrophilic ones, nontoxic and biodegradable	Clinical MRI	[130]
MRI contrast agents for the breast cancer	4–12 nm	Thermal decomposition/nanocrystals	Strong MR signals, biocompatible, minimal nonspecific adhesion of the conjugates with excellent selectivity	Cancer diagnosis, high-performance magnetic nanocrystal probe systems	[199]
Ultra sensitive magnetic resonance probe	8–16 nm	Co-precipitations/clustered micelles	Drastically increasing the image contrast, ultra sensitive towards MRI	Therapeutic and clinical diagnostic applications, probing	[199]

magnetization (Ms) of 78.75 emu/g leads to new potential applications such as high-density recording media magnetic sensors [139]. Monodisperse magnetic-plasmonic Fe_3O_4-Au/porous silica core/shell nanoparticles, with nanoporous silica shells containing both primary and secondary amine groups, demonstrate a significant interest for coupling biomolecules. The multifunctional nanoarchitectures could also offer an ultimate platform to study the molecules with low fluorescence efficacies, and exhibit promising potential in practical applications such as multimodal imaging, bio sensing, or localized drug delivery [140]. Fe_3O_4–NH_2/PEI-EDTA has been proven to be an effective, rapid and convenient nano-adsorbent for the removal of heavy metal ions (such as Cu^{2+}, $Pb^{2+}$and Cd^{2+}) from aqueous solutions [141]. Magnetic sedimentation and magnetophoresis have been used for separation purposes, generally in combination with magnetically loaded colloids or cells in the micrometer range [142].

In data storage applications, the particles must have a stable, switchable magnetic state that is not be affected by temperature fluctuations [143]. For optimum performance in recording, the particles should exhibit both high coercivity and high remanence, and they should be uniformly small, and resistant to corrosion, friction, and temperature changes [144]. It was also found that the biotinylated PNIPAAm-coated iron oxide nanoparticles can still bind to the surface of a streptavidin-coated sensor chip with high affinity proving it valuable for therapeutic applications in biotechnology and biomedicines [110].

The NBR/nano-Fe_3O_4 composites show good anti-wear and friction-reducing properties. The nano-Fe_3O_4 is conducive to forming physical adsorption film and self-repairing film on the friction surface. It has the effect of improving the resistance to wear and friction. Clearly, the addition of nano Fe_3O_4 particles can improve friction and wear performance of NBR, and is helpful for its application in sealing [145].

Maghemite is useful in recording and data storage applications because of its chemical and physical stability [146]. It is often doped or coated with 1–5% cobalt in order to improve its coercivity and storage capacity. Coated nanoparticles have greater thermal stability than their doped counterparts and display uniaxial magnetic anisotropy [41].

Internalization of iron oxide particles strongly depends upon the size of the particles [147]. After administration, larger particles with a diameter higher than 200 nm are easily sequestered by the spleen and eventually removed by the cells of the phagocyte system, resulting in decreased blood circulation times. Magnetic drug targeting employing nanoparticles as carriers is a promising cancer treatment avoiding the side effects of conventional chemotherapy [148]. The incorporation of radioisotopes enables testing and describing the nanometerscale delivery vehicles for medical diagnostic and therapeutic purposes [149].

Layer-by-layer films of hemoglobin with magnetic Fe_3O_4 nanoparticles were successfully assembled on various solid surfaces mainly by electrostatic interaction between them. The good biocatalytic activity of Hb incorporated in multilayered $\{Fe_3O_4/Hb\}_6$ films toward various substrates may establish a foundation for fabricating the new kind of biosensors or bioreactors without using chemical mediators [150].

Superparamagnetic iron oxide nanoparticles play an important role as MRI contrast agents, to better differentiate healthy and pathological tissues. Recent developments in MR imaging have enabled in vivo imaging at near microscopic resolution [151]. In order to visualize and track stem and progenitor cells by MR imaging, it is necessary to tag cells magnetically. Tat protein-derived peptide sequences have recently been used as an efficient way of internalizing a number of marked proteins into cells [152].

Some of the most important merits reported by different authors are given in the Table 2 given below.

Commercialized SPIONs

Superparamagnetic iron oxide nanoparticles (SPIO-NPs) have traditionally been used as MRI contrast agent for disease imaging via passive targeting [153]. However, there has been an increasing interest in the development of SPIO-NPs to cellular-specific targeting for imaging and drug delivery currently [32]. Due to rapidly growing applications in different fields of life different type of spions are commercially available [154]. Superparmagnetic magnetite nanoparticles can be applied to microbead applications of a biosensor [155].

Table 3 given below shows different SPIONs and its application with the reference of companies those are commercializing them [156].

Table 3 Different SPIONs available commercially and their applications

Company	Applications	References
Stemcell Technologies	Automated immunomagnetic cell separation	www.stemcell.com
Chemicell	Bioseparation- and detection systems	www.chemicell.com
Diagnostics Biosensors	Diagnostics biosensors	www.diagnosticbiosensors.com
Micromod	Biomagnetic separation, nucleic acid purification, drug delivery	www.micromod.de
Ocean Nanotech	R&D of magnetic NPs	www.oceannanotech.com
Imego	Medical diagnostics	www.imego.com
Integrated Engineering Software	Electromechanical and electrothermal analysis software	www.integratedsoft.com
EMD chemicals	Immunoassay and immunoreagent development	www.emdchemicals.com
TurboBeads	Magnetic separation	www.turbobeads.com
European Institute of Science	Hyperthermia	www.biotechniques.com
nanoTherics Ltd	Magnetic gene transfection	www.nanotherics.com
SEPMAG technologies	Magnetic separation systems	www.sepmag.eu
Estapor	Immunoassays	www.estapor.com

Conclusion

In conclusion, Iron oxide magnetic nanoparticles can be designed to exhibit novel and significantly improved physical, chemical and biological properties, phenomena and strategies as a result of the limited size of their constituent particles by using above stated methodologies. This review reveals that Magnetic iron oxide NPs, especially superparamagnetic (SPM) NPs, is attractive magnetic probes for biological imaging and therapeutic applications. The examples illustrated in table further demonstrate that magnetic nanoparticles made from chemical synthesis with controlled size, surface chemistry and magnetic properties are indeed promising for further ultra-high density information storage, highly sensitive medical diagnostics and highly efficient therapeutic applications. The USPIONs appear to be nontoxic, are easy to manage, and provide substantial contrast enhancement, even on low tesla magnets. They may serve as complimentary agents to increase localization, characterization, and addition in different neurologic lesions. In CNS tumors, USPIONs may improve diagnosis and detection at early stages and will be of much significance in the future for monitoring therapeutic responses to antiangiogenic chemotherapies. There is a lot of activity in this field, and the future is bright, so long as we pay attention to the primary criteria for success, making sure that there is a clearly identified clinical need that can be addressed. It may also be prudent to carefully assess the potential applications for any new approach to see whether there is a simple, straightforward target that may be addressed in the short term.

Acknowledgements The authors would like to acknowledge the support provided by the Deanship of Scientific Research (DSR) at King Fahd University of Petroleum and Minerals (KFUPM) for funding this work through project No. SR161009. Project No. SR161009 has been awarded to Dr. Muhammad Ramzan Saeed Ashraf Janjua who is working as a Principal Investigator (PI) in this project. He is also thankful to his parent university, University of Sargodha (UOS) where he has been working since November 2010 on regular basis at BPS 19. He has been doing his research in KFUPM as an Assistant Professor of Physical Chemistry since January 2016 after taking permission and Ex-Pakistan Extra-Ordinary Leave (EOL) from Department of Chemistry, University of Sargodha, Pakistan. This research publication is the result of joint venture of UOS and KFUPM.

References

1. A. Pankhurst, J. Connolly, S. K. Jones, and J. Dobson (2003). *J. Phys. D Appl. Phys.* **36**, R167–R181.
2. C. B. Catherine and S. G. C. Curtis (2003). *J. Phys. D Appl. Phys.* **36**, R198–R206.
3. S. Chikazumi, S. Taketomi, M. Ukita, M. Mizukami, H. Miyajima, M. Setogawa, and Y. Kurihara (1987). *J. Magn. Magn. Mater* **65**, 245.
4. A.-H. Lu, W. Schmidt, N. Matoussevitch, H. Bönnemann, B. Spliethoff, B. Tesche, E. Bill, W. Kiefer, and F. Schüth (2004). *Angew. Chem.* **116**, 4403.
5. A. C. Tsang, V. Caps, I. Paraskevas, D. Chadwick, and D. Thompsett (2004). *Angew. Chem.* **116**, 5763.
6. A. K. Gupta and M. Gupta (2005). *Biomaterials* **26**, 3995–4021.
7. S. Mornet, F. Vasseur, P. Grasset, G. Verveka, A. Goglio, J. Demourgues, E. Portier, E. Pollert, and E. Duguet (2006). *Prog. Solid State Chem.* **34**, 237.
8. Z. Li, L. Wei, M. Y. Gao, and H. Lei (2005). *Adv. Mater.* **17**, 1001.
9. T. Hyeon (2003). *Chem. Commun.* **8**, 927.

10. D. W. Elliott and W.-X. Zhang (2001). *Environ. Sci. Technol.* **35**, 4922.
11. M. Takafuji, S. Ide, H. Ihara, and Z. Xu (2004). *Chem. Mater* **16**, 1977.
12. A. H. Lu, E. L. Salabas, and F. S. Angew (2007). *Chem. Int. Ed.* **46**, 1222–1244.
13. C. Xu and S. Sun (2007). *Polym. Int.* **56**, 821–826.
14. S. S. Lee, J. Park, Y. Chung, and H. B. Na (2001). *J. Am. Chem. Soc.* **123**, 12798–12801.
15. B. H. Sohn and R. E. Cohen (1997). *Chem. Mater.* **9**, 264.
16. D. K. Kim, Y. Zhang, W. Voit, K. V. Rao, and M. Muhammed (2001). *J. Magn. Magn. Mater.* **225**, 30–36.
17. J. Gao, H. W. Gu, and B. Xu (2009). *Acc. Chem. Res.* **42**, 1097–1107.
18. L. Wang, H. Y. Park, S. I.-I. Lim, M. J. Schadt, D. Mott, J. Luo, X. Wang, and C.-J. Zhong (2008). *J. Mater. Chem.* **18**, 2629–2635.
19. Y. Lu, Y. Yin, B. T. Mayers, and X. Younan (2002). *Nano Lett.* **2**, 183–186.
20. Q. A. Pankhurst, N. K. T. Thanh, S. K. Jones, and J. Dobson (2010). *Acta Elct. Et. Info.* **10**, 39–42.
21. P. Berger, N. B. Adelman, K. J. Bechman, D. J. Campbell, A. B. Ellis, and G. C. Lisensky (1999). *J. Chem. Educ.* **76**, 943.
22. C. Y. Wang, G. M. Zhu, Z. Y. Chen, and Z. G. Lin (2002). *Mater. Res. Bull.* **37**, 2525.
23. B. Fang, G. Wang, W. Zhang, M. Li, and X. Kan (2005). *Electroanalysis* **17**, 744–748.
24. S. Laurent, D. Forge, M. Port, A. Roch, C. Robic, L. V. Elst, and R. N. Muller (2008). *Chem. Rev.* **108**, 2064–2110.
25. A. E. Gash, T. M. Tillotson, J. H. Satcher, J. F. Poco, L. W. Hrubesh, and R. L. Simpson (2001). *Chem. Mater.* **13**, 999–1007.
26. M. N. Berger (2007). *Acc. Chem. Res.* **40**, 793–800.
27. S. M. Moghimi, A. C. H. Hunter, and J. C. Murray (2001). *Pharm. Rev.* **53**, 283–318.
28. J. M. Wilkinson (2003). *Med. Device Technol.* **14**(5), 29–31.
29. R. K. Gilchrist, R. Medal, W. D. Shorey, R. C. Hanselman, J. C. Parrot, and C. B. Taylor (1957). *Ann. Surg.* **146**, 596–606.
30. L. Babes, B. Denizot, G. Tanguy, J. J. Le Jeune, and P. Jallet (1999). *J. Colloid Int. Sci.* **212**, 474–482.
31. W. Wu, Q. He, and C. Jiang (2008). *Nanoscale Res. Lett.* **3**, 397–415.
32. Y. H. Zheng, Y. Cheng, F. Bao, and Y. S. Wang (2006). *Mater. Res. Bull.* **41**, 525–529.
33. T. Ozkaya, M. S. Toprak, A. Baykala, H. Kavas, Y. Köseoğlu, and B. Aktas (2009). *J. Alloys Compd.* **472**, 18–23.
34. J. Wang, J. Sun, Q. Sun, and Q. Chen (2003). *Mater. Res. Bull.* **38**, 1113–1118.
35. S. Si, C. Li, X. Wang, D. Yu, Q. Peng, and Y. Li (2005). *Cryst. Growth Des.* **5**, (2), 391–393.
36. H. W. Wang, H. Lin, Y. C. Yeh, and C. H. Kuo (2007). *J. Magn. Magn. Mater.* **310**, 2425–2427.
37. Z. L. Liu and X. Wang (2004). *J. Mater. Sci.* **39**, 2633–2636.
38. S. Ni, S. Lin, Q. Pan, F. Yang, K. Huang, and D. He (2009). *J. Phys. D Appl. Phys.* **42**, 055004–0550016.
39. F. Dang, K. Kamada, N. Enomoto, J. Hojo, and K. Enpuku (2007). *Ceram. Soc. J.* **115**(12), 867–872.
40. A.-L. Morel, S. I. Nikitenko, K. Gionnet, A. Wattiaux, J. Lai-Kee-Him, C. La-brugere, B. Chevalier, G. Deleris, C. Petibois, A. Brisson, and M. Simonoff (2008). *ACSNANO.* **5**(2), 847–856. doi:10.1021/nn800091q.
41. N. Wang, L. Zhu, D. Wanga, M. Wang, Z. Lin, and H. Tang (2010). *Ultrason. Sonochem.* **17**, 526–533.
42. A. Yan, X. Liu, G. Qiu, and H. Wu (2008). *J. Alloys. Compd.* **458**, 487–491.
43. R. A. Mukh-Qasem and A. Gedanken (2005). *J. Colloid Interface Sci.* **284**(2), 489–494.
44. R. A. Mukh-Qasem and A. Gedanken (2008). *J. Phys. Chem.* **112**, 35–42.
45. M. N. Islam, L. V. Phong, J. Jeong and C. Kim (2011). *Thin Solid Films* in press.
46. Z. Mo, C. Zhang, R. Guo, S. Meng, and J. Zhang (2011). *Ind. Eng. Chem. Res.* **50**, 3534–3539.
47. A. Zhua, L. Yuan, and T. Liao (2008). *Int. J. Pharm.* **350**, 361–368.
48. M. Titirici, M. Antonietti, and A. Thomas (2006). *Chem. Mater.* **18**, 3808–3812.
49. S. Sun* and H. Zeng (2002). *J. Am. Chem. Soc.* **124**(28), 8204–8205.
50. A. B. Chin and I. I. Yaacob (2007). *J. Mater. Proces. Technol.* **191**, 235–237.
51. R. Honga, J. Li, J. Wang, and H. Li (2007). *China Particuol.* **5**, 186–191.
52. H. T. Chana, Y. Y. Doa, P. L. Huanga, P. L. Chienb, T. S. Chanc, R. S. Liuc, C. Y. Huangd, S. Y. Yangd, and H. E. Horngd (2006). *J. Magn. Magn. Mater.* **304**, e415–e417.
53. H. Zeng, J. Li, Z. L. Wang, J. P. Liu, and S. Sun (2004). *Nano Lett.* **4**(2), 187–190.

54. Y. Lu, Y. Yin, B. T. Mayers, and Y. Xia (2002). *Nano Lett.* **2**(3), 3183–3186.
55. S. Santra, R. Tapec, N. Theodoropoulou, J. Dobson, A. Hebard, and W. Tan (2001). *Langmuir* **17**, 2900–2906.
56. S. Park, S. Kim, S. Lee, Z. G. Khim, K. Char, and T. Hyeon (2000). *J. Am. Chem. Soc.* **122**, 8581–8582.
57. R. Zboril (2002). *Chem. Mater.* **14**, 969–982.
58. K. Woo, J. Hong, S. Choi, H.-W. Lee, J.-P. Ahn, C. S. Kim, and S. W. Lee (2004). *Chem. Mater.* **16**, 2814–2818.
59. B. Bourlinos, A. Bakandritsos, V. Georgakilas, and D. Petridis (2002). *Chem. Mater.* **14**, 3226–3228.
60. R. V. Kumar, Y. Diamant, and A. Gedanken (2000). *Chem. Mater.* **12**, 2301–2305.
61. R. A. Mukh-Qasem and A. Gedanken (2005). *J. Colloid Interface Sci.* **284**, 489–494.
62. M. N. Islam, L. V. Phong, J. R. Jeong, and C. G. Kim (2011). *Thin Solid Films* in press.
63. K. Nishioa, M. Ikedaa, N. Gokonb, S. Tsubouchia, H. Narimatsua, Y. Mochizukia, S. Sakamotoa, A. Sandhuc, M. Abe, and H. Handa (2007). *J. Magn. Magn. Mater.* **310**, 2408–2410.
64. J. Qiu, H. Peng, and R. Liang (2007). *Electrochem. Commun.* **9**, 2734–2738.
65. Z. Huang and F. Tang (2004). *J. Colloid Interface Sci.* **275**, 142–147.
66. Z. Lu, G. Wang, J. Zhuang, and W. Yang (2006). *Physicochem. Eng. Asp.* **278**, 140–143.
67. A. Jordan, R. Scholz, P. Wust, H. Fakhling, and R. Felix (1999). *J. Magn. Magn. Mater.* **201**, 413–419.
68. E. E. Carpenter (2001). *J. Magn. Magn. Mater.* **225**, 17–20.
69. Z. Z. Xu, C. C. Wang, W. L. Yang, Y. H. Deng, and S. K. Fu (2004). *J. Magn. Magn. Mater.* **277**, 136–143.
70. M. Hofmann and B. V. Rechenberg (2005). *J. Magn. Magn. Mater.* **293**, 483–496.
71. Y. C. Chang and D. H. Chen (2005). *J. Colloid Interface Sci.* **283**, 446–451.
72. C. H. Peng, H. W. Wang, S. W. Kanb, M. Z. Shenb, Y. M. Weib, and S. Y. Chena (2004). *J. Magn. Magn. Mater.* **284**, 113–119.
73. D. K. Kim, Y. Zhang, W. Voit, K. V. Rao, J. Kehr, B. Bjelke, and M. Muhammed (2001). *Scr. Mater.* **44**, 1713–1717.
74. S. W. Kamau, S. Katja, P. F. Alke, H. Paul, H. Michael, H. Heinrich, and H. Margarethe (2005). *Eur. J. Cell Mater.* **10**, 10.
75. J. Lim, C. Lanni, E. R. Evarts, F. L. Robert, and S. A. Majetich (2011). *ACS Nano* **5**(1), 217–226.
76. Y. Lu, Y. Yin, B. T. Mayers, and Y. Xia (2002). *Nano Lett.* **2**(4), 183–186.
77. F. Erogbogbo, K. T. Yong, R. Hu, W. C. Law, H. Ding, C. W. Chang, P. N. Prasad, and M. T. Swihart (2010). *ACS* **4**(9), 5131–5138.
78. T. K. Jain, M. K. Reddy, M. A. Morales, D. L. Leslie-Pelecky, and V. Labhasetwar (2008). *Mol. Pharm.* **5**(2), 316–327.
79. P. Sun, H. Zhang, C. Liu, J. Fang, M. Wang, J. Chen, J. Zhang, C. Mao, and S. Xu (2010). *Langmuir* **26**, (2), 1278–1284.
80. C. Yee, G. Kataby, A. Ulman, T. Prozorov, H. White, A. King, M. Rafailovich, J. Sokolov, and A. Gedanken (1999). *Langmuir* **15**, 7111–7115.
81. E. Taboada, E. Rodríguez, A. Roig, J. Oró, A. Roch, and R. N. Muller (2007). *Langmuir* **23**, 4583–4588.
82. A. J. Rondinone, A. C. S. Samia, and Z. J. Zhang (1999). *J. Phys. Chem.* **103**, 6876–6880.
83. H. Duan, M. Kuang, X. Wang, Y. A. Wang, H. Mao, and S. Nie (2008). *J. Phys. Chem. C* **112**(22), 8127–8131.
84. D. Tang, R. Yuan, and Y. Chai (2006). *J. Phys. Chem.* **110**, 11640–11646.
85. G. Zou, K. Xiong, C. Jiang, H. Li, T. Li, J. Du, and Y. Qian (2005). *J. Phys. Chem.* **109**, 18356–18360.
86. S. Li, Y. C. Hong, H. S. Uhm, and Z. Li (2004). *Jpn. J. Appl. Phys.* **43**(11A), 7714–7717.
87. M. Chen, S. Yamamuro, D. Farrell, and S. A. Majeticha (2003). *J. Appl. Phys.* **93**(10), 7551–7553.
88. Y. Deng, D. Qi, C. Deng, X. Zhang, and D. Zhao (2008). *J. Am. Chem. Soc.* **130**, 28–29.
89. Y.-W. Jun, Y.-M. Huh, J.-S. Choi, J.-H. Lee, H.-T. Song, and S. Kim (2005). *J. Am. Chem. Soc.* **127**, 5732–5733.
90. S. X. Wang and G. Li (2004). *J. Am. Chem. Soc.* **126**, 273–279.
91. S. Sun, S. Anders, H. F. Hamann, J.-U. Thiele, J. E. E. Baglin, T. Thomson, E. E. Fullerton, C. B. Murray, and B. D. Terris (2002). *J. Am. Chem. Soc.* **124**(12), 2884–2885.

92. J.-P. Fortin, C. Wilhelm, J. Servais, C. Ménager, J.-C. Bacri, and F. Gazeau (2007). *J. Am. Chem. Soc.* **129**, 2628–2635.
93. W. Zhao, J. Gu, L. Zhang, H. Chen, and J. Shi (2005). *J. Am. Chem. Soc.* **127**, 8916–8917.
94. A. Dyal, K. Loos, M. Noto, S. W. Chang, C. Spagnoli, K. V. P. M. Shafi, A. Ulman, M. Cowman, and R. A. Gross (2003). *J. Am. Chem. Soc.* **125**, 1684–1685.
95. S. D. Dickson, W. Chen, A. W. Griffioen, Z. A. Fayad, W. J. M. Mulder, and P. A. Jarzyna (2009). *Biomaterials* **30**, 6947–6954.
96. S. A. Corr, P. Y. Rakovich, and Y. K. Gu'nko (2008). *Nanoscale Res. Lett.* **3**, 87–104.
97. J. Gao, H. Gu, and B. Xu (2009). *Acc. Chem. Res.* **42**(8), 1097–1107.
98. E. Alphandéry, Y. Ding, A. T. Ngo, Z. L. Wang, L. F. Wu, and M. P. Pileni (2009). *ACS Nano* **3**(6), 1539–1547.
99. H. Zhang, M.-Y. Lee, M. G. Hogg, J. S. Dordick, and S. T. Sharfstein (2010). *ACS Nano* **4**(8), 4733–4743.
100. M. Fröba, R. Köhn, and G. Bouffaud (1999). *Chem. Mater.* **11**, 2858–2865.
101. B. K. Pradhan, T. Toba, T. Kyotani, and A. Tomita (1998). *Chem. Mater.* **10**, 2510–2515.
102. G. Ennas, A. Musinu, G. Piccaluga, and D. Zedda (1998). *Chem. Mater.* **10**, 495–502.
103. A. S. Teja and P.-Y. Koh (2009). *Prog. Cryst. Growth Charact. Mater.* **55**, 22–45.
104. X. Zhao, Y. Cai, T. Wang, Y. Shi, and G. Jiang (2008). *Anal. Chem.* **80**, 9091–9096.
105. F. M. Kievit, F. Y. Wang, C. Fang, H. Mok, K. Wang, J. R. Silber, R. G. Ellenbogen, and M. Zhang (2011). *J. Control. Release* in press.
106. J. Xie, K. Chen, J. Huang, S. Lee, J. Wang, J. Gao, X. Li, and X. Chen (2010). *Biomaterials* **31**, 3016–3022.
107. F. Dilnawaz, A. Singh, C. Mohanty, and S. K. Sahoo (2010). *Biomaterials* **31**, 3694–3706.
108. P. Girginova, A. L. Daniel-da-Silva, C. B. Lopes, P. Figueira, M. Otero, V. S. Amaral, E. Pereira, and T. Trindade (2010). *J. Colloid Interface Sci.* **345**, 234–240.
109. I. Koh, X. Wang, B. Varughese, L. Isaacs, S. H. Ehrman, and D. S. English (2006). *J. Phys. Chem.* **110**, 1553–1558.
110. Z. Yuanbi, Q. Zumin, and H. Jiaying (2008). *Chin. J. Chem. Eng.* **16**(3), 451–455.
111. J.-I. Jo, I. Aoki, and Y. Tabata (2010). *J. Control. Release* **142**, 465–473.
112. C. Xu, K. Xu, H. Gu, R. Zheng, H. Liu, X. Zhang, Z. Guo, and B. Xu (2004). *J. Am. Chem. Soc.* **126**, 9938–9939.
113. C. Fan, W. Gao, Z. Chenc, H. Fan, M. Li, F. Deng, and Z. Chen (2011). *Int. J. Pharm.* **404**, 180–190.
114. I. De Vicentea, A. Merino-Martos, L. Cruz-Pizarroa, and J. de Vicentec (2010). *J. Hazard. Mater.* **181**, 375–381.
115. K. Chen, J. Xie, H. Xu, D. Behera, M. H. Michalski, S. Biswal, A. Wang, and X. Chen (2009). *Biomaterials* **30**, 6912–6919.
116. N. Tran and T. J. Webster (2011). *Acta Biomater.* **7**, 1298–1306.
117. O. Lunov, T. Syrovets, B. Büchele, X. Jiang, C. Röcker, K. Tron, G. U. Nienhaus, P. Walther, V. Mailänder, K. Landfester, and T. Simmet (2010). *Biomaterials* **31**, e5063–e5071.
118. B. Zargar, H. Parham, and A. Hatamie (2009). *Chemosphere* **76**, 554–557.
119. F. Yang, Y. Li, Z. Chen, Y. Zhang, J. Wu, and N. Gu (2009). *Biomaterials* **30**, 3882–3890.
120. A. Azhari, F. Golestani-Fard, and H. Sarpoolaky (2009). *J. Eur. Ceram. Soc.* **29**, 2679–2684.
121. A. Figuerola, R. D. Coratob, L. Manna, and T. Pellegrino (2010). *Pharmacol. Res.* **62**, 126–143.
122. M. Mahmoudi, S. Sant, B. Wang, S. Laurent, and T. Sen (2011). *Adv. Drug Deliv. Rev*. in press.
123. S. Cheng, J.-H. Jang, B. A. Dempsey, and B. E. Logan (2011). *Water. Res.* **45**, 303–307.
124. H. Lee, E. Lee, D. K. Kim, N. K. Jang, Y. Y. Jeong, and S. Jon (2006). *J. Am. Chem. Soc.* **128**, 7383–7389.
125. R. Y. Honga, B. Feng, L. L. Chen, G. H. Liu, H. Z. Li, Y. Zheng, and D. G. Wei (2008). *Biochem. Eng. J.* **42**, 290–300.
126. R. Narain, M. Gonzales, A. S. Hoffman, P. S. Stayton, and K. M. Krishnan (2007). *Langmuir* **23**, 6299–6304.
127. N. A. Frey, S. Peng, K. Cheng, and S. Sun (2009). *Chem. Soc. Rev.* **38**(9), 2532–2542.
128. D. Cao and N. Hu (2006). *Biophys. Chem.* **121**, 209–217.
129. T. K. Jain, M. A. Morales, S. K. Sahoo, D. L. Leslie-Pelecky, and V. Labhasetwar (2005). *Mol. Pharm.* **2**(3), 194–205.
130. F. Sonvico, S. Mornet, S. Vasseur, C. Dubernet, D. Jaillard, J. Degrouard, J. Hoebeke, E. Duguet, P. Colombo, and P. Couvreur (2005). *Bioconjugate Chem.* **16**, 1181–1188.

131. J. Fuliu, Z. Shanzhao, and A. Binjiang (2008). *Environ. Sci. Technol.* **42**, 6949–6954.
132. M. Mikhaylova, D. K. Kim, C. C. Berry, A. Zagorodni, M. Toprak, A. S. G. Curtis, and M. Muhammed (2004). *Chem. Mater.* **16**, 2344–2354.
133. S. Q. Wang, C. R. Li, Y. M. Miao, Z. Y. Wu, and B. S. Zou (2005). *J. Phys. D Appl. Phys.* **38**, 1342–1350.
134. P. Tartaj, M. P. Morales, S. Veintemillas-Verdaguer, T. González-Carreño, and C. J. Serna (2003). *J. Phys. D Appl. Phys.* **36**, R182–R197.
135. H. Wei and E. Wang (2008). *Anal. Chem.* **80**, 2250–2254.
136. G. K. Kouassi and J. Irudayaraj (2006). *Anal. Chem.* **78**, 3234–3241.
137. A. Tsukamoto, K. Saitoh, D. Suzuki, N. Sugita, Y. Seki, A. Kandori, K. Tsukada, Y. Sugiura, S. Hamaoka, H. Kuma, N. Hamasaki, K. Enpuku, and I. E. E. E. Trans (2005). *Appl. Supercond.* **15**(2), 656–659.
138. D.-L. Zhao, H.-L. Zhang, X.-W. Zeng, Q.-S. Xia, and J.-T. Tang (2006). *Biomed. Mater.* **1**, 198–201.
139. J. Li and H. Gao (2008). *Electroanalysis* **20**(8), 881–887.
140. A. Erdem, F. Sayar, H. Karadeniz, G. Guven, M. Ozsoz, and E. Piskinb (2007). *Electroanalysis* **19**(7–8), 798–804.
141. I.-M. Hsing, Y. Xu, and W. Zhao (2007). *Electroanalysis* **19**(7–8), 755–768.
142. B. Fang, G. Wang, W. Zhang, M. Li, and X. Kan (2005). *Electroanalysis* **17**(9), 744–748.
143. Q. A. Pankhurst, N. K. T. Thanh, S. K. Jones, and J. Dobson (2009). *J. Phys. D Appl. Phys.* **42**, 224001–224016.
144. M. Irama, C. Guo, Y. Guan, A. Ishfaq, and H. Liu (2010). *J. Hazard. Mater.* **181**, 1039–1050.
145. S. Tanaka, C. Toriyabe, Y. Torii, Y. Hatsukade, T. Eki, S. Katsura, N. Ohnishi, J. Wan, S. Yang, and Y. Zhang (2007). *Phys. C: Supercond Appl.* **463–465**, 1029–1033.
146. L. Zhou, R. Diao, T. Zhou, H. Wang, H. Kage, and Y. Mawatari (2010). *Adv. Powder Technol.* in press.
147. Z. M. Saiyed, C. Bochiwal, H. Gorasia, S. D. Telang, and C. N. Ramchand (2006). *Anal. Biochem.* **356**, 306–308.
148. M. Xu, Y. Zhang, Z. Zhang, Y. Shen, M. Zhao, and G. Pan (2011). *Chem. Eng. J.* **168**, 737–745.
149. Y. F. Shen, J. Tang, Z. H. Nie, Y. D. Wang, Y. Ren, and L. Zuo (2009). *Sep. Sci. Technol.* **68**, 312–319.
150. Q. Wei, Z. Xiang, J. He, G. Wang, H. Li, Z. Qian, and M. Yang (2010). *Biosens. Bioelectron.* **26**, 627–631.
151. B. Chertok, B. A. Moffat, A. E. David, F. Yu, C. Bergemann, B. D. Ross, and V. C. Yang (2008). *Biomaterials* **29**, 487–496.
152. C. Sun, J. S. H. Lee, and M. Zhang (2008). *Adv. Drug Deliv. Rev.* **60**, 1252–1265.
153. C. H. Dodd, H.-C. Hsu, W.-J. Chu, P. Yang, H.-G. Zhang, J. D. Mountz Jr., K. Zinn, J. Forder, L. Josephson, R. Weissleder, J. M. Mountz, and J. D. Mountz (2001). *J. Immunol. Methods* **256**, 89–105.
154. Q. Wang, F. Yang, Q. Yang, J. Chen, and H. Guan (2010). *Mater. Des.* **31**, 1023–1028.
155. U. T. Lam, R. Mammucari, K. Suzuki, and N. R. Foster (2008). *Ind. Eng. Chem. Res.* **47**, 599–614.
156. X. F. Zhang, L. Clime, H. Q. Ly, M. Trudeau, and T. Veres (2010). *J. Phys. Chem. C* **114**, 18313–18317.
157. J. Fang, H. Wang, Y. Xue, X. Wang, T. Lin, and A. C. S. Appl (2010). *Mater. Interfaces* **2**(5), 1449–1455.
158. T. K. Jain, M. A. Morales, S. K. Sahoo, D. L. Leslie-Pelecky, and V. Labhasetwar (2010). *Mol. Pharm.* **2**(3), 194–205.
159. H. Chen, X. Wu, H. Duan, Y. A. Wang, L. Wang, M. Zhang, H. Mao, and A. C. S. Appl (2009). *Mater. Interfaces* **1**(10), 2134–2140.
160. V. Zelenak, A. Zelenakova, J. Kovac, U. Vainio, and N. Murafa (2009). *J. Phys. Chem. C* **113**, 13045–13050.
161. U. O. Häfeli, J. S. Riffle, L. Harris-Shekhawat, A. Carmichael-Baranauskas, F. Mark, J. P. Dailey, and D. Bardenstein (2009). *Mol. Pharm.* **6**(5), 1417–1428.
162. D. Ma, T. Veres, L. Clime, F. Normandin, J. Guan, D. Kingston, and B. Simard (2007). *J. Phys. Chem. C* **111**, 1999–2007.
163. Y. Xu, A. Karmakar, D. Wang, M. W. Mahmood, F. Watanabe, Y. Zhang, A. Fejleh, P. Fejleh, Z. Li, G. Kannarpady, S. Ali, A. R. Biris, and A. S. Biris (2010). *J. Phys. Chem. C* **114**, 5020–5026.
164. Z. Lei, N. Ren, Y. Li, N. Li, and B. Mu (2009). *J. Agric. Food Chem.* **57**, 1544–1549.

165. S. Xuan, F. Wang, J. M. Y. Lai, K. W. Y. Sham, Y.-X. J. Wang, S.-F. Lee, J. C. Yu, C. H. K. Cheng, and K. C.-F. Leung (2011). *ACS Appl. Mater. Interface* **3**, 237–244.
166. F. Bertorelle, C. Wilhelm, J. Roger, F. Gazeau, C. Ménager, and V. Cabuil (2006). *Langmuir* **22**, 5385–5391.
167. M. A. M. Gijs, F. Lacharme, and U. Lehmann (2010). *Chem. Rev.* **110**, 1518–1563.
168. Y. Zhai, J. Zhai, Y. Wang, S. Guo, W. Ren, and S. Dong (2009). *J. Phys. Chem. C* **113**, 7009–7014.
169. S. T. Selvan, T. T. Yang Tan, D. K. Yi, and N. R. Jana (2010). *Langmuir* **26**(14), 11631–11641.
170. N. Insin, J. B. Tracy, H. Lee, J. P. Zimmer, R. M. Westervelt, and M. G. Bawendi (2008). *ACS Nano* **2**(2), 197–202.
171. E. S. M. Lee, J. Chan, B. Shutter, L. Tan, M. S. K. Chong, D. L. Ramachandra, G. S. Dawe, J. Ding, S. H. Teoh, O. Beuf, A. Briguet, K. C. Tam, M. Choolani, and S. Wang (2009). *Stem Cells* **27**, 1921–1931.
172. S. Wang, Y. Tan, D. Zhao, and G. Liu (2008). *Biosens. Bioelectron.* **23**, 1781–1787.
173. A. Erdem, F. Sayar, H. Karadeniz, G. Guven, M. Ozsoz, and E. Piskin (2007). *Electroanalysis* **19**, 798–804.
174. E. Katz, I. Willner, and J. Wang (2004). *Electroanalysis* **16**, 1–2.
175. W. Zhao, J.-J. Xu, and H.-Y. Chen (2006). *Electroanalysis* **18**, 1737–1748.
176. J. Liu, J. Liu, L. Yang, X. Chen, M. Zhang, F. Meng, T. Luo, and M. Li (2009). *Sensors* **9**, 7343–7364.
177. A. El-Ansary and L. M. Faddah (2010). *Nano Technol.* **3**, 65–76.
178. A. Ansari, M. Alhoshan, M. S. Alsalhi, and A. S. Aldwayyan (2010). *Sensors* **10**, 6535–6581.
179. G. Ning, W. Lu-Yan, L. Tian-Hua, Z. Lei, and W. Feng (2009). *Chin. J. Anal. Chem.* **37**(8), 1125–1130.
180. U. Yogeswaran, S. Thiagarajan, and S.-M. Chen (2008). *Sensors* **8**, 7191–7212.
181. K.-S. Loh, Y. H. Lee, A. Musa, A. A. Salmah, and I. Zamri (2008). *Sensors* **8**, 5775–5791.
182. W. Wen, Y. Tan, H. Xiong, and S. Wang (2010). *Int. J. Electrochem. Sci.* **5**, 232–241.
183. J. Wang, A. Munir, Z. Zhu, and H. S. Zhou (2010). *Anal. Chem.* **82**, 6782–6789.
184. G. Zhao, J.-J. Feng, Q.-L. Zhang, S.-P. Li, and H.-Y. Chen (2005). *Chem. Mater.* **17**, 3154–3159.
185. Z. Li, J. F. Godsell, J. P. O'Byrne, N. Petkov, M. A. Morris, S. Roy, and J. D. Holmes (2010). *J. Am. Chem. Soc.* **132**, 12540–12541.
186. S. H. Gee, Y. K. Hong, D. W. Erickson, and M. H. Park (2003). *J. Appl. Phys.* **93**(10), 7560–7562.
187. L. Machala, R. Zboril, and A. Gedanken (2007). *J. Phys. Chem.* **111**, 4003–4018.
188. J. Zhou, X. Qiao, B. P. Binks, K. Sun, M. Bai, Y. Li, and Y. Liu (2011). *Langmuir* **27**, 3308–3316.
189. T.-L. Zhang and B.-H. Han (2010). *Langmuir* **26**(11), 8893–8900.
190. L. Yang, X. Ren, F. Tang, and L. Zhang (2009). *Biosens. Bioelectron.* **25**, 889–895.
191. H. Zhu, J. Han, J. Q. Xiao, and Y. Jin (2008). *J. Environ. Monit.* **10**(6), 685–784.
192. Q. Lan, C. Liu, F. Yang, S. Liu, J. Xu, and D. Sun (2007). *J. Colloid Interface Sci.* **310**, 260–269.
193. R. Zhang, X. Wang, C. Wu, M. Song, J. Li, G. Lv, J. Zhou, C. Chen, Y. Dai, F. Gao, D. Fu, X. Li, Z. Guan, and B. Chen (2006). *Nano. Technol.* **17**, 3622–3626.
194. B.-L. Lin, X.-D. Shen, and S. Cui (2007). *Biomed. Mater.* **2**, 132–134.
195. H. Lee, M. K. Yu, S. Park, S. Moon, J. J. Min, Y. Y. Jeong, H.-W. Kang, and S. Jon (2007). *J. Am. Chem. Soc.* **129**(42), 12739–12745.
196. H.-L. Duan, Z.-Q. Shen, X.-W. Wang, F.-H. Chao, and J.-W. Li (2005). *World J. Gastroenterol.* **11**(24), 3660–3664.
197. Y. F. Shen, J. Tang, Z. H. Nie, Y. D. Wang, Y. Ren, and L. Zuo (2009). *Sep. Purif. Technol.* **68**, 312–319.
198. J. Wang, Z. Zhu, A. Munir, and H. S. Zhou (2011). *Talanta* **84**, 783–788.
199. V. Chandra, J. Park, Y. Chun, J. Woo Lee, I. Hwang, and K. S. Kim (2010). *ACS Nano* **4**(7), 3979–3986.